Optimising the formation of WO_{3-x} nanostructures: stars, fibres and spheres

M. Govender[1, 2], L. Shikwambana[1, 2], B. W. Mwakikunga[1], E. Sideras-Haddad[2, 3], R. M. Erasmus[2] and A. Forbes[1, 4]

[1] CSIR National Laser Centre, P. O. Box 395, Pretoria 0001, South Africa

[2]School of Physics, University of the Witwatersrand, Private Bag 3, P. O. Wits 2050, Johannesburg, South Africa

[3]iThemba Labs, Private Bag 11, Wits 2050, Jan Smuts and Empire Road, Johannesburg

[4]School of Physics, University of KwaZulu-Natal, Private Bag X54001, Durban 4000, South Africa

Abstract We report on the production of multi-phase WO_3 and WO_{3-x} (where x could vary between 0.2 and 0.33) nanostructures synthesized by CO_2-laser pyrolysis technique at varying laser wavelengths (9.22-10.82 μm) and power densities (17-110 W/cm^2). The average spherical particle sizes for the wavelength variation samples ranged between 113-560 nm and the average spherical particle sizes for the power density variation samples ranged between 108-205 nm. Synthesis of W_3O_8 (= $WO_{2.67}$) stars by this method is reported for the first time at a power density and wavelength of 2.2 kW/cm^2 and 10.6 μm, respectively. It was found that more concentrated starting precursors result in the growth of hierarchical structures such as stars, whereas dilute starting precursors result in the growth of simpler structures such as wires.

Introduction

Tungsten trioxide is known as a "smart material" because it exhibits excellent electrochromatic, photochromatic and gasochromatic properties. Nano-sized tungsten trioxide

has been applied in many nano-photonic devices for applications such as photo-electro-chromic windows [1], sensor devices [2-3] and optical modulation devices [4]. Many techniques for synthesizing nano-sized tungsten trioxide have been reported [5-8] and here we concern ourselves with laser pyrolysis. Laser pyrolysis is advantageous over most methods because the experimental orientation does not allow the reactants to make contact with any side-walls, so the products are of high quality and purity [9]. Laser pyrolysis is based on photon-induced chemical reactions, which is believed to rely on a resonant interaction between a laser beam's emission line and a precursor's absorption band, such that a photochemical reaction is activated [10]. The photochemical reaction enables an otherwise inaccessible reaction pathway toward a specific product, either by dissociation, ionization or isomerisation of the precursor compound. It was shown [8, 11] that low laser power densities can also achieve the same products as the high power densities, presumably due to the way photon-energy is distributed into the energy levels of the precursor.

In this Letter, we report for the first time on the formation of W_3O_8 (= $WO_{2.67}$) stars and the effect of laser power and wavelength on the morphological and structural properties of tungsten trioxide nanostructures and thin films.

Experimental

The laser pyrolysis experimental setup was discussed in detail in [10], and a schematic description of the experiment during laser-precursor interaction is depicted in Fig. 1. The laser pyrolysis method is carried out within a custom-made stainless steel chamber at atmospheric pressure. A wavelength tunable continuous wave (CW) CO_2 laser was used in the experiments (Edinburgh Instruments, PL6) and the beam was focused into the reaction chamber with a 1 m radius of curvature concave mirror (copper coated, II-IV Inc.) which is effectively a lens with a focal length of 500 mm. For low power densities, an unfocused beam was used by replacing the concave mirror with a flat mirror (copper coated, II-IV Inc.). An IR-detector (Spiricon PY-III-C-A) was used to trace out the laser beam profile at various propagation distances from the flat or concave mirror to determine the beam properties. The laser power was varied using a polarization based attenuator, and the wavelength variation was achieved with an intra-cavity mounted grating in the laser. The different wavelengths were identified with a spectrum analyzer (Macken Instruments, model 16A) and the power output was measured with a power meter (Coherent Inc.).

The synthesis of WO_3 and WO_{3-x} commenced by mixing 0.1 g of greyish-blue anhydrous tungsten hexachloride WCl_6 (Aldrich 99.9%) powder in 100 mL of absolute ethanol C_2H_5OH (Aldrich 99.9%) to give a tungsten ethoxide $W(OC_2H_5)_6$ starting precursor [12]. Optical absorption properties of the precursor were determined using a Perkin Elmer Spotlight 400 FTIR Imaging System in the wavelength range 500-4000 cm^{-1}. The liquid precursor was decanted into an aerosol generator (Micro Mist, model EN) which was attached to the laser pyrolysis system via a multiflow nozzle that allows argon gas to carry the stream of very fine precursor droplets (~5 μm droplet diameter according to the manufacturer) into the laser beam. Acetylene (C_2H_2) sensitizer gas and argon encasing gas flowed adjacent to the precursor, guiding it towards a substrate. The gas flow rates are chosen such that the ablated precursor collects on the substrate after interacting with the laser. The sample was annealed for 17 hours at 500^oC under argon atmosphere [10]. Morphology studies were carried out using a Jeol JSM-5600 Scanning Electron Microscopy (SEM) microscope (using the secondary electron mode). Raman spectroscopy was carried out using a Jobin-Yvon T64000 Raman Spectrograph with a wavelength of 514.5 nm from an argon ion laser set at a laser power of 0.384 mW at the sample, in order to minimize local heating of the sample during the Raman analysis. X-ray diffraction (XRD) was carried out using a Philips Xpert powder diffractometer equipped with a Cu K_α wavelength of 154.184 pm. The reproducibility of the experimental procedure was not verified.

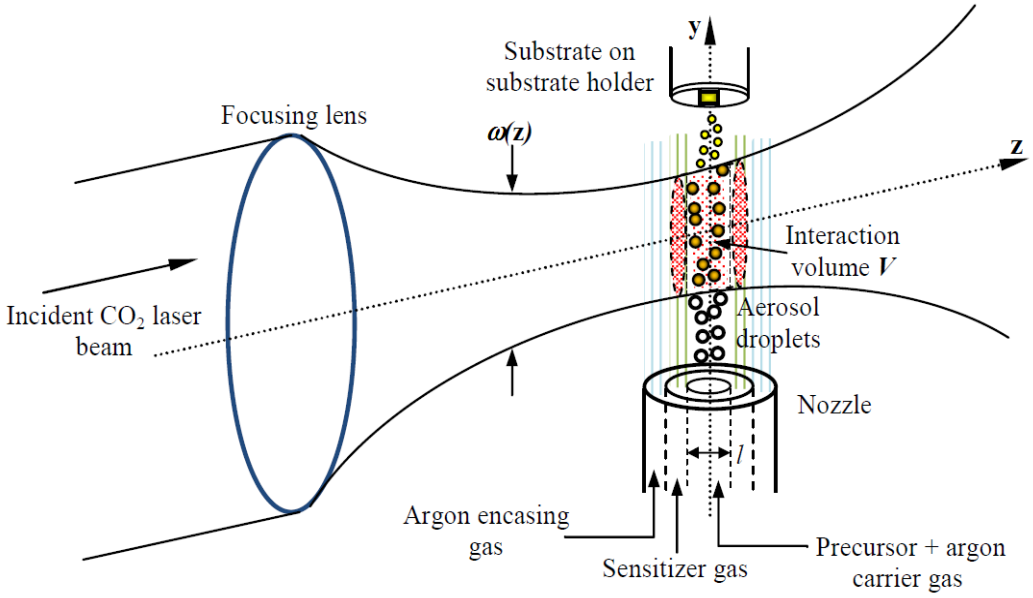

Fig. 1 A schematic of laser pyrolysis within the reaction chamber during laser-precursor interaction

Results

When the CO_2 laser beam was focused with a 1 m radius of curvature mirror, it gave a minimum beam radius or beam waist of 1.2 mm, and at a laser power of 50 W on the 10.6 μm emission line, a power density of 2.2 kW/cm^2 was achieved. These parameters were consistent with those used to synthesize WO_3 nanowires using a very dilute precursor of 27 μM [10]. Laser pyrolysis of the more concentrated 2.5 mM precursor showed many uniform agglomerations composed of nanospheres (~40 nm) prior to annealing, as depicted in the SEM micrograph in the inset of Fig. 2. The sample was annealed and from the agglomerates grew stars with six points as seen in the SEM micrographs of Fig. 2.

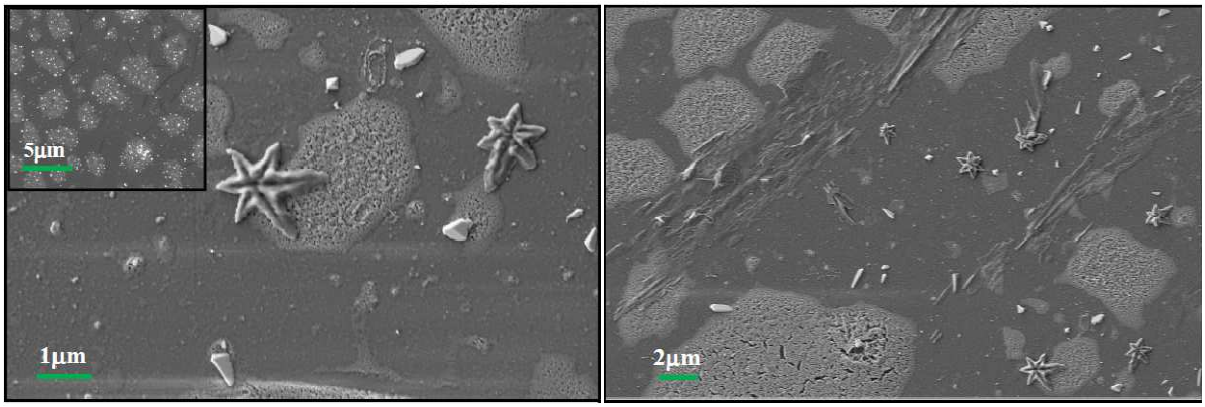

Fig. 2 Scanning electron micrographs of the post-annealed sample showing the growth of six-sided stars from the agglomerations of the pre-annealed sample depicted in the inset

The Raman and XRD spectra of the samples containing the stars are shown in Fig. 3. The stars were not visible under the Raman microscope so various spots were analyzed on the sample. The Raman study shows that the sample is amorphous after annealing, and the lack of a dominant peak at ~800 cm^{-1} suggests the absence of monoclinic phase tungsten trioxide and possibly an oxygen deficiency [13-14]. The Raman peaks found near 224 cm^{-1}, 288 cm^{-1} and 320 cm^{-1} is indicative of a W-O-W stretching mode of a tungsten oxide. The Raman peak at 700 cm^{-1} is designated to the bridging O-W-O vibrations in tungsten trioxide and the asymmetry in this phonon peak shows that there are a number of phonons confined in the tungsten oxide layer of particles. This indicates that the product is composed of particles less than 20 nm in size [15-16]. The peak near 960 cm^{-1} is assigned to the W^{6+}=O symmetric stretching mode. The XRD studies revealed weak peaks at the 23 and 24 degrees diffraction angle which suggests a tungsten oxide compound, but the lack of a triplet peak confirms the absence of monoclinic tungsten trioxide. The broad hump at ~22 degrees resulted from SiO_2

of the substrate, and this substantially decreased the signal-to-noise ratio making it difficult to identify the peaks. XRD peaks at the 12, 40 and 64 degrees diffraction angles are also evident in tungsten oxides but the 44 degree diffraction angle suggests that the tungsten oxide has a deficiency of oxygen [18]. Based on the information from Raman spectroscopy and XRD, the most probable stoichiometry of this sample is orthorhombic phase W_3O_8 (= $WO_{2.67}$). According to the Powder Diffraction File (PDF 81-2263) that best matches the XRD spectrum in Fig. 3, the lattice constants *a*, *b* and *c* are 10.35 Å, 13.99 Å and 3.78 Å, respectively and the lattice angles are all equal to 90^o. The Miller indices are shown on the XRD spectrum in Fig. 3.

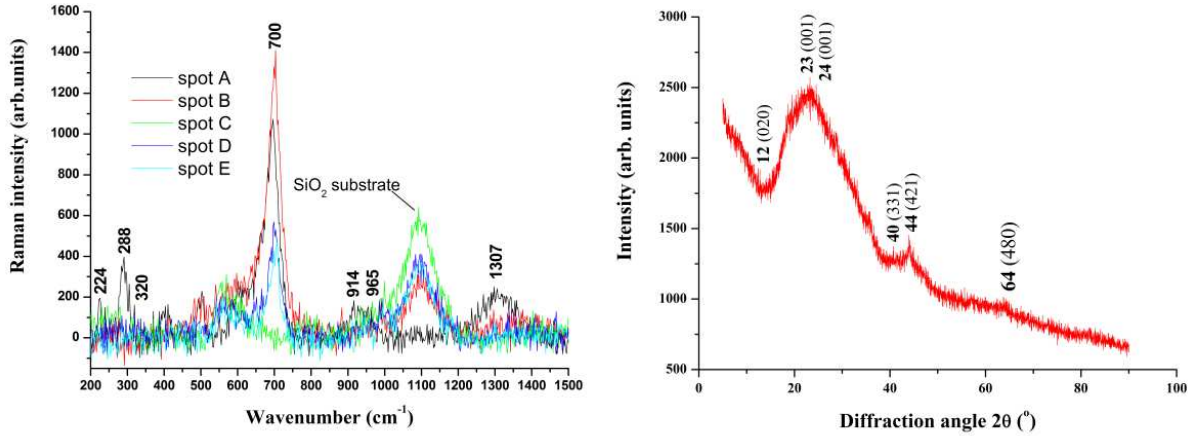

Fig. 3 *Left*: Raman spectrum and *Right*: XRD spectrum of the sample containing the stars

Previously solid-vapour-solid (SVS) [8] and solution-liquid-solid (SLS) [19] mechanisms were proposed to explain the growth of nanowires of tungsten trioxide and platinum, respectively. Since the tungsten trioxide nanowires were grown with a low precursor concentration using a similar laser beam and laser parameters, the precursor concentration is seemingly the main contributor to hierarchical structure growth. This was confirmed by the 100 times more concentrated precursor that was used for the growth of stars. The six-sided stars that were grown in Fig. 2 looked very similar to lead (II) sulphide (PbS) stars that were grown by a concentration difference and gradient (CDG) technique [20]. This CDG technique used a high local concentration of one reactant mixed with a low concentration of another reactant under ambient conditions, where the high concentration favoured the thermodynamic conditions for crystal growth and the low concentration resulted in a diffusion-controlled kinetic environment for growth of hierarchical structures. It is possible that due to a Gaussian

laser beam profile, which has a high intensity at the beam's centre and low intensity at the edges, the region of intensity in the beam experienced by the precursor, could vary the concentration of the decomposed material. We speculate that this variation in concentration could have led to the growth of the hierarchical structures according to the CDG technique. The growth of stars has also been reported before for gold, lead and molybdenum oxide [21-22], but not as yet for tungsten oxide. The literature proposes that star-shaped structures can be grown from agglomerates of more simple nanoforms under an inert atmosphere, which were similar conditions for this experiment [21-22]. One growth mechanism of nanostructures could be due to Gibbs-Thompson effect [23-25], which proposes that the size of the critical radius is dependent on the precursor concentration and explains the increase (Ostwald ripening) or decrease (Tiller's formula) in size of nanostructures. The higher concentration probably provided a critical radius which resulted in simple nanoforms and the growth of stars as opposed to a lower concentration which resulted in microspheres and the growth of wires. We speculate that the critical radius influences the thermodynamic and kinetic conditions as predicted by the CDG technique. Thus the laser beam properties together with the relative precursor concentration contribute to the growth of stars. Some stars may form with four-sides and others with six-sides depending on the crystalline plane arrangement and the elements composing the structures [20]. It is not yet understood if the observed deficiency of oxygen plays a role in the formation of the six-sided stars or if the higher tungsten content, with a predominant valency of +6, has some correlation with the number of sides formed.

It is thought that acetylene gas acts as a photosensitizer [10] in laser pyrolysis, yet we have found no evidence of absorption in the laser wavelength range 9.19-10.82 μm. This was verified by passing the acetylene gas through the laser beam and monitoring the power change during this interaction. The laser power did not appear to show any change which implied that no radiation was absorbed by this gas. This does not however, discount the possibility of some short-lived metastable state in acetylene induced by the laser which was undetectable by the power meter. The argon-precursor mixture however, showed a change in power which indicated that the radiation was being absorbed, and the maximum absorbance was found at a wavelength of 9.54 μm. The absorbance of the precursor was given by the ratio of the laser power before laser-precursor interaction to the power observed during laser-precursor interaction. Fig. 4 shows the absorbance by the precursor as a function of

wavelength with the corresponding part of the FTIR transmission spectrum of tungsten ethoxide. This assists in determining if the laser pyrolysis mechanism is a resonant process or if the precursor is decomposed by collisions with excited photosensitizer molecules. The results indicate that the laser energy is transferred to the precursor and should cause decomposition by a resonant process, thus leading to the formation of the predicted products. Thus acetylene probably provides a reducing atmosphere in the laser-precursor interaction that influences the reaction pathway towards the formation of the products.

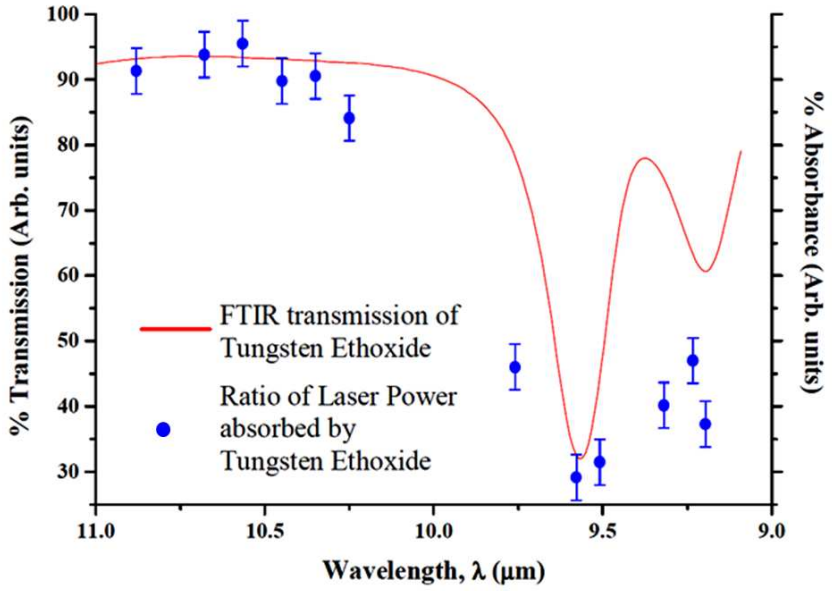

Fig. 4 The comparison of the FTIR transmittance spectrum of the tungsten ethoxide precursor and the CO_2 laser radiation absorbance data of tungsten ethoxide as a function of wavelength

To determine how the laser wavelength plays a role in laser pyrolysis, it was varied between 9.19-10.82 μm at a constant power of 30 W and power density of 51.2 W/cm^2. The lower power density was achieved by replacing the focusing mirror with a flat mirror to obtain a beam radius of 6.11 mm. The low power density was chosen such that all the *R*- and *P*-branches of the CO_2 laser supplied a constant power output for the varying wavelengths. It was also assumed that at such low power density, minimum heating effects are involved in the laser-precursor interaction. It was found that only the 10.48 μm wavelength formed monoclinic phase WO_3 according to the Raman and XRD spectra shown in Fig. 5 with the corresponding SEM micrograph. The nanosphere diameters of this sample were distributed in the range 50-250 nm as depicted in inset of Fig 5 and there were also micron-sized fibres

present in this sample. The theory speculates that if the laser wavelength is resonant with the C-O absorption band of the precursor (W-O-C_2H_5), the C-O bond would break and lead to the formation of tungsten oxide. Since FTIR showed that the C-O absorption band is found between 9.00-9.38 µm (see Fig. 4), and despite argon carrier gas presumably broadening the precursor absorption bands to some extent [26], the result could refer to a non-resonant energy transfer. A 10.48 µm wavelength photon carries ~0.1 eV of energy, so ~29 photons are required to dissociate a C-O bond [27] which refers to a multi-photon process. It is known however, that tungsten ethoxide precursor can form WO_3 upon heat treatment [12], which implies that the 10.48 µm wavelength could have had similar effects than annealing. We believe that the shorter wavelengths, which had higher energy photons, dissociated various bonds which led to the formation of tetragonal phase WO_{3-x} where x can vary between 0.2 and 0.33, depending on the laser parameters. It was also observed that the morphology of the samples became more random and of a disordered arrangement as the wavelength increased, and we believe this to be an effect of a corresponding decrease in energy.

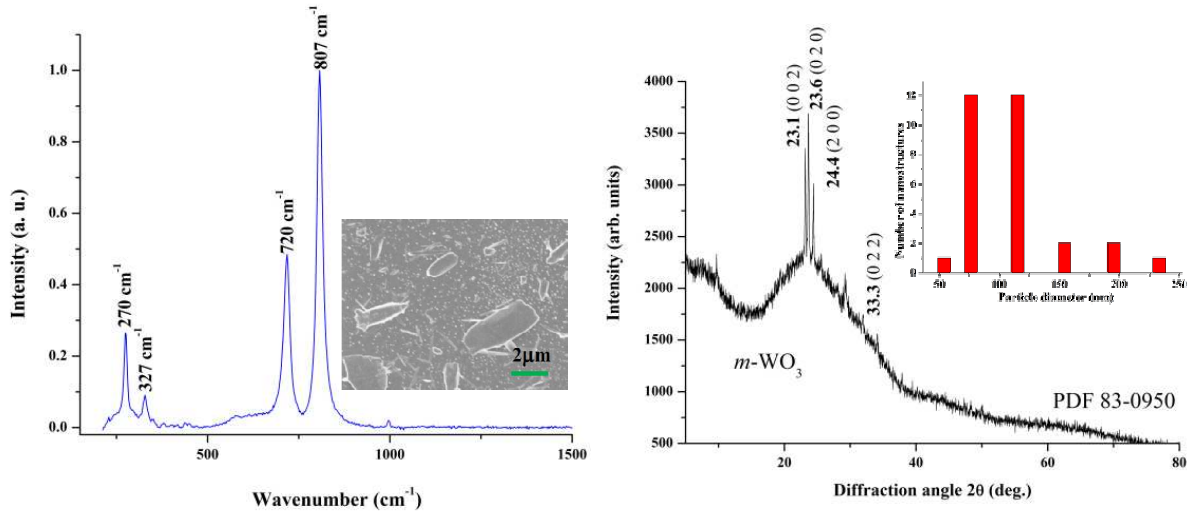

Fig. 5 *Left*: The Raman spectrum of the sample prepared at the 10.48 µm wavelength and 51.2 W/cm^2 power density with a SEM micrograph in the inset showing the morphology and *Right*: the corresponding XRD spectrum with the histogram of the diameters of a selection of the nanostructures of the corresponding SEM micrograph in the inset. The Raman and XRD spectra suggest a monoclinic phase WO_3.

Unlike the increasing wavelength, the increase in power density led to more ordered and shaped nanostructures, presumably due to the increase in energy rate. Furthermore, it was

observed that at high enough power densities, it was more likely for nanostructure growth to take place. At such low power densities (17-110 W/cm^2) on the 10.6 µm wavelength, the particle sizes did not show a decrease with increasing power density as predicted [28] for the higher power density range (1-100 kW/cm^2). The nanosphere diameters of this sample were found to be in the range 150-400 nm as depicted in inset of Fig 6. It was observed that the overall particle sizes were smaller for the power variation experiment while the wavelength variation experiment showed larger particle sizes. The increase in power density did not always favour the formation of WO_3, and since the photon energy was constant, only the number of photons per unit time varied. Fig 6 shows the Raman and XRD spectra with the corresponding SEM micrograph of a sample prepared at a power density of 85 W/cm^2 at the 10.6 µm wavelength that appeared to form a tetragonal phase WO_3 according to the characteristic peaks.

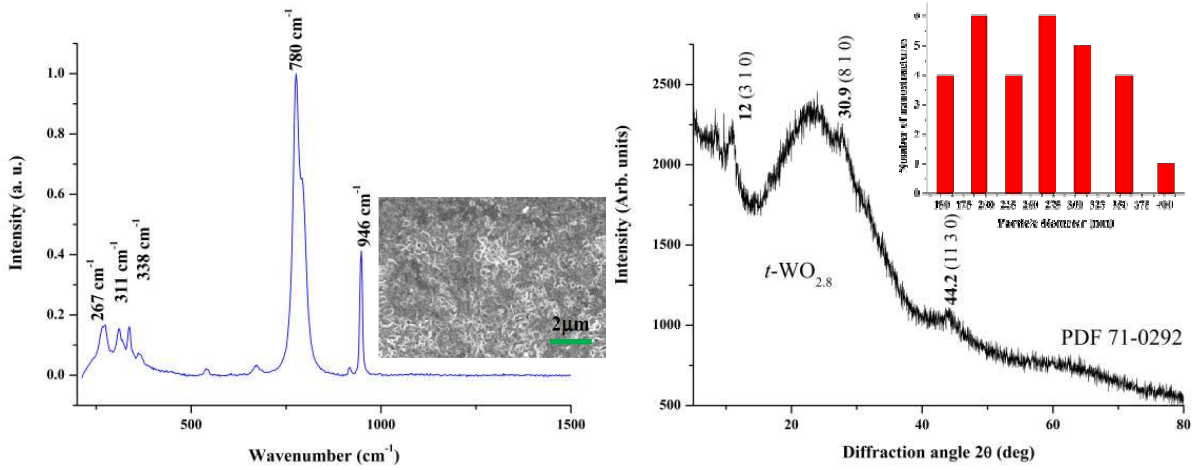

Fig. 6 *Left*: The Raman spectrum of the sample prepared at the 10.6 µm wavelength and 85 W/cm^2 power density with a SEM micrograph in the inset showing the morphology and *Right*: the corresponding XRD spectrum with the histogram of the diameters of a selection of the nanostructures of the corresponding SEM micrograph in the inset. The Raman and XRD spectra suggest a tetragonal phase WO_{3-x} (x~0.2).

Table 1 summarizes all the results obtained for the varying laser parameters. The average particle sizes observed for the wavelength variation was in the range 113-560 nm while the average particle sizes for the power density variation was in the range 108-205 nm. The compositions of some samples were uncertain so it is written as WO_{3-x} where x most likely attains values between 0.2 and 0.33 according to the corresponding powder diffraction files.

There were no obvious trends as to how the laser parameters affected the product size or composition and thus we believe there is some possible competing reactions taking place during the laser-precursor interaction or during annealing.

Table 1 A summary of the results obtained for the laser power and wavelength variation

Wavelength Variation ($P_{density}$ = 51.2 W/cm^2)			Power Density Variation (λ = 10.6 μm)		
Wavelength, λ (μm)	*Average sphere particle size (nm)*	*Composition*	*Power Density, P_{peak} (W/cm^2)*	*Average sphere particle size (nm)*	*Composition*
9.22	343	*t*-WO_{3-x}	17	157	*t*-WO_{3-x}
9.32	125	*t*-WO_{3-x}	26	122	*t*-WO_{3-x}
9.48	113	*t*-WO_{3-x}	34	140	*m*-WO_3
9.70	403	*t*-WO_{3-x}	43	193	*m*-WO_3
10.16	360	*t*-WO_3	51	108	*t*-WO_3
10.36	560	*t*-WO_3	60	122	*t*-WO_{3-x}
10.48	347	*m*-WO_3	68	136	*m*-WO_3
10.82	453	*o*-WO_3	77	180	*m*-WO_3
			85	205	*t*-WO_{3-x}
			94	114	*o*-WO_3
			100	106	*m*-WO_3
NB. *m* refers to monoclinic phase, *o* refers to orthorhombic phase and *t* refers to tetragonal phase.			110	128	*m*-WO_3
			2200	100	*o*-$WO_{2.67}$

Conclusion

Six-sided orthorhombic phase $WO_{2.67}$ stars were synthesized by laser pyrolysis technique using a more concentrated starting precursor and near-Gaussian laser beam profile. The higher concentrated precursors are required to obtain hierarchical structures as predicted by literature. Laser wavelengths above 10 μm seem to favor the formation of stoichiometric WO_3, but only at certain power densities, presumably to overcome possible competing

reactions. Due to the nature of photochemical reactions and the many stoichiometries and multi-phases that tungsten oxides can form, some product compositions were written as WO_{3-x} where x most probably assumes values between 0.2 and 0.33. The higher power densities were found to be essential for the further growth of structures and for a smaller particle sizes. We now have an idea of the possible shapes of nanostructures that can be synthesized with possible chemical compositions and the determination of the electrical and optical properties of these structures to observe possible unique characteristics allows for the tailoring of sensor devices that operate at room temperature for example.

References

1. C. Bittencourt, R. Landers, E. Llobet, G. Molas, X. Correig, M. A. P. Silva, J. E. Sueiris, and J. Calderer, Electrochem. Soc. **149**, H81 (2002)

2. H. Kawasaki, J. Namba, K. Iwatsuji, Y. Suda, K. Wada, K. Ebihara, and T. Ohshima, Applied Surface Science, **197-198**, 547-551 (2002)

3. V. Guidi et al., Sens. Actuators B **100**, 277 (2004)

4. S. W. Wang, T. C. Chou, and C. C. Liu, Sens. Actuators B **94**, 343 (2003)

5. X. P. Wang, B. Q. Yang, H. X. Zhang, and P. X. Feng, Nanoscale Res Lett **2**, 405-409 (2007)

6. S Rajagopal, D Nataraj, D Mangalaraj, Y. Djaoued, J. Robichaud, and O Khyzhun, Nanoscale Res Lett **4**, 1335-1342 (2009)

7. B. W. Mwakikunga, A. Forbes, E. Sideras-Haddad, M. Scriba, and E. Manikandan, Nanoscale Res Lett **5**, 389-397 (2010)

8. B. W. Mwakikunga, A. Forbes, E. Sideras-Haddad, and C. Arendse, Nanoscale Res Lett **3**, 372-380 (2008)

9. J. S. Haggerty and W. R. Cannon, New York: Plenum Press, 165-241 (1981)

10. B. W. Mwakikunga, A. Forbes, E. Sideras-Haddad, R. M. Erasmus, G. Katumba, and B. Masina, Int. J. Nanoparticles **1**, 185-200 (2008)

11. C. M. Bowden, J. D. Stettler, N. M. Witriol, J. Phys. B Atom. Mol. Phys. **10**, 1789 (1977)

12. S. Sakka, *Handbook of sol-gel science and technology: processing, characterization and applications*, Boston: Kluwer Academic Publishers (2004)

13. D. Y. Lu, J. Chen, J. Zhou, S. Z. Deng, N. S. Xu and J. B. Xu, J. Raman Spectrosc. **38**, 176-180 (2007)

14. D. Y. Lu, J. Chen, S. Z. Deng, N. S. Xu, W. H. Zhang, J. Mater. Res., Vol. 23, No. 2, 402-408 (2008)

15. B. W. Mwakikunga, E. Sidera-Haddad, A. Forbes and C. Arndse, Phys. Stat. Sol. (a) **205**, No. 1, 150-154 (2004)

16. A. K. Arora, M. Rajalakshmi, T. R. Ravindran, Encyclopedia of Nanoscience and Nanotechnology, Edited by H. S. Nalwa Volume X: Pages (1–13) (2003)

17. R. Ganesan and A. Gedanken, Nanotechnology **19** (2008)

18. www.surechem.org, "Microelectronic capacitor with capacitor plate layer formed of tungsten rich tungsten oxide material", Patent number: 6456482, (2002)

19. J. Chen, B. J. Wiley, and Y. Xia, Langmuir **27**, 4120-4129 (2007)

20. H. Chu, X. Li, G. Chen, Z. Jin, Y. Zhang and Y. Li, Nano Res 1:213-220 (2008)

21. O. V. Kharissova, B. I. Kharisov, T. H. García, and U. O. Méndez, Synthesis and Reactivity in Inorganic, Metal-Organic, and Nano-Metal Chemistry **39**, 662-684 (2009)

22. A. Khademi, R. Azimirad, A. A. Zavarian, and A. Z. Moshfegh, *J. Phys. Chem. C* **44**, 19298–19304 (2009)

23. J. S. Haggerty and W. R. Cannon, New York: Plenum Press, 165-241 (1981)

24. W. Qin-bo, R. Finsy, X. Hai-bo, L. Xi, J Zhejiang Univ 6B(8),705-707 (2005)

25. W. A. Tiller, *The science of crystallization: Microscopic interfacial phenomenon*, Cambridge University Press, New York (1991)

26. F. El-Diasty, Optics Communications **241**, 121-135 (2004)

27. G. Glockler, J. Phys. Chem, 62 (9) 1049-1054 (1959)

28. O. Bomatí-Miguel, X. Q. Zhao, S. Martelli, P. E. Di Nunzio, and S. Veintemillas-Verdaguer, J. Appl. Phys. **107**, 014906 (2010)